*Metrol. Meas. Syst.*, Vol. 31 (2024) No. 3, pp. 577–594
DOI: 10.24425/mms.2024.150289

PAN POLSKA AKADEMIA NAUK

METROLOGY AND MEASUREMENT SYSTEMS

Index 330930, ISSN 0860-8229
*www.metrology.wat.edu.pl*

M&MS

# MEASUREMENT SYSTEMS OF ELECTROMAGNETIC FIELD FOR AIRCRAFT WITH THE USE OF A MACHINE LEARNING MODEL

**Joanna Michałowska[1)], Paweł Tomiło[2)]**

*1) Department of Electrical Engineering and Superconductivity Technologies, Lublin University of Technology, 38A Nadbystrzycka Street, 20-618 Lublin, Poland* (✉ *jmichalowska@panschelm.edu.pl*)
*2) Faculty of Management, Lublin University of Technology, 38 Nadbystrzycka Street, 20-618 Lublin, Poland*

**Abstract**

In this article, a new low-cost measurement system for measuring the electric component of electromagnetic field is presented. For the initial calibration of the new measurement system, a reference meter was used, and based on its readings, calibration was carried out using a machine learning model. Initial calibration was carried out in a GTEM 1000 with a Teseq ITS 6006 generator connected. Five models were compared, among which the K-Nearest Neighbors (KNN) model had the highest accuracy. The model was tested on 5 types of aircraft, and its readings were compared with a reference sensor. Test measurements were carried out in five types of aircraft: Cessna C172, Aero AT-3 R100, Tecnam P2006T, PZL M28 Bryza and the Mi-8 helicopter with the developed new measurement system and a reference meter (NHT3DL) with an 01E probe. The new measurement system is small in size and fits anywhere in the aircraft cockpit. To compare the models, the following metrics were used: the coefficient of determination, mean absolute error, mean square error and root mean square error. The Two-sample Kolmogorov-Smirnov tests were used for analysis, and the Bag of Words and Bag of Patterns methods were applied.

Keywords: electromagnetic field (EMF), aircraft, measurement system, Machine Learning Model (MLM).

## 1. Introduction

The impact of electromagnetic field on human body and on electronic devices is the subject of interest in many research centers around the world. Speculations on the effects of positive and negative impacts are the subject of research that has been confirmed in many publications [1–4].

Petroulakis *et al.*, [5] in their research work presented integrated sensors for monitoring and assessing radio frequencies in the context of exposure to electromagnetic fields and human health. They conducted a four-year research project dedicated to monitoring and analyzing the impact of electromagnetic fields on human health. They demonstrated that research and monitoring of electromagnetic field are important knowledge that will be used in further scientific work.



Article history: received March 5, 2024; revised May 30, 2024; accepted June 5, 2024; available online June 27, 2024.

Mallik *et al.* [6] created a neural network model called EMGAN - for the reconstruction of electromagnetic field propagation in an urban environment. They collected measurement data from several sensors placed in Lille, France. They showed the EMGAN algorithm learns and uses information about the propagation of radio waves in the environment in a much more accurate manner than experimental data obtained from traditional field measurements.

Subsequently, Silva *et al.* [7] measured the electromagnetic field in a shopping mall in Natal, Brazil. They proposed a set of 6 measurement points that occur in places with large concentrations of people and at least in the vicinity of one *distributed antenna system* (DAS). It was shown that the strongest electric field was 3.4 V/m, which is 8% of the limit set by the *International Commission on Non Ionizing Radiation Protection* (ICNIRP). The authors emphasized the fact that neither scientists nor the *World Health Organization* (WHO) issued any global conclusion on the harmful impact of non-ionizing radiation on human health, therefore prevention is always necessary.

In turn, Bae *et al.* [8] in their work examined the assessment of exposure to electromagnetic fields generated by electric car chargers. The assessment was based on the ICNIRP. It has been shown that magnetic field increases with charging current, which contributes to the charging speed. The highest measurement values were 46 A/m. It was noted that the permissible limits set by ICNIRP were not exceeded.

However, Atanasova [9] conducted research on exposure to electromagnetic field inside a car while driving. They measured electromagnetic fields in cars during short (between cities) and long (between countries) trips on several European roads in Austria, Bulgaria, Croatia, Hungary, Italy, Slovenia and the Republic of Serbia. They showed that the highest measurement values were achieved during a trip across Austria ($E$ = 17.4 V/m).

Current literature reports include research on the development of various types of cheap sensors to monitor phenomena related to health and the entire environment. Based on such analyses, appropriate recommendations regarding the use of such devices appear [10–15]. In [10], a simple low-cost capacitive pressure sensor was developed. It has been shown to have a wide range of applications, excellent repeatability of results, and high sensitivity. In turn, in [11] an innovative, inexpensive measurement system composed of a sensor node that uses economical electrochemical sensors to measure the concentration of carbon monoxide (CO) and nitrogen dioxide ($NO_2$) as well as an infrared sensor to measure the level of *particulate matter* (PM) has been proposed. It has been shown that the use of cheap sensors allows using a network of serial sensors to measure air pollution in real time in a large number of locations. In contrast, air quality monitoring stations are often limited to a small number of locations due to the high cost of monitoring equipment. It was shown that the data from low-cost sensors, with the offset correction and gain calibration, correlates well with the data acquired from the reference sensor. The work [11] presents the measurement system of an inexpensive, innovative *air pollution monitoring device* (APMD). The obtained results were verified with reference measurements performed using a professional, expensive measuring instrument. To build the measurement system, there were used an operational amplifier, a microcontroller, a brushless DC motor, a photodetector, and sensors. Measurement data were collected locally and also sent to the IoT cloud platform. It was shown that the measurement data read from the developed system differ from the reference data. A machine learning model was proposed for sensor calibration. It was shown that the optimized multi-sensor prototype module was 90.8% more energy efficient in the long run in comparison with the reference design. An innovative, cheap measurement system consisting of an EVAL-AD5933EBZ evaluation board housing an AD5933 IC for measuring the water surface level is presented in [12]. It was shown that maximum errors of 6.1% and 5.6% were obtained for capacitance and conductivity, respectively.

Machine learning methods are quite often used in the calibration of various types of devices [16–18]. This kind of calibration is carried out in a supervised learning manner, so the low-cost sensor data are related to that of the reference sensor. Machine learning models are able to take non-linearity into account, so they can outperform linear models in a significant way. In [18] Park, D *et al.* showed that the proposed neural network model using machine learning solves the existing limitations of the accuracy of cheap sensors and can provide high-reliability results not only for monitoring, but also for research in various fields of environmental protection. It has been shown that due to the use of neural networks, high measurement accuracy can be achieved using cheap PM 2.5 sensors for measuring suspended dust.

Monitoring electromagnetic field in an aircraft may have many benefits. It is particularly related to the safety of both people and avionics systems. Based on extensive research conducted by the research team, which began in 2018 [19–22] and on the basis of the conclusions drawn, it resulted in the need to design and built a new low-cost system to measure electromagnetic field. Analyzing the physical nature of electromagnetic phenomena, various variants of a proprietary measurement system were developed. The obtained measurement characteristics of the measurement system were correlated with the reference measurement equipment.

The aim of the present study was to develop a new low-cost measurement system for measuring the effective value of the electric component of electromagnetic field in the aircraft cockpit. Measurements and data acquisition of field parameters involve the use of expensive measuring devices. Typically, measurement capabilities are reduced due to high cost. The development of a new measurement system together with a data acquisition system will enable measurements to be carried out at selected points in the vicinity of field sources. The developed measurement system is particularly suitable for conducting measurements aimed at determining both the exposure of aircraft operators and avionics equipment, which directly translates into flight safety. The development of such a relatively simple and cheap device will allow measurements to be performed by pilots and aircraft crew members in order to quantitatively determine what field environment they are exposed to. The data obtained by measurement in the field of electromagnetic fields will ensure the availability of results to both the scientific community and society, as well as regulatory organizations. Performing such measurements using devices that may become widely available due to their low cost will also increase public awareness.

Therefore, we can describe the contribution of this study as follows:

– designing and implementing a measurement system consisting of an antenna, a power detector, a microcontroller and a smartphone,

– developing a new model based on a machine learning algorithm, which will serve as a calibration model for the developed measurement system,

– developing an original data acquisition system,

– preparing and conducting airfield experiments with five different aircraft,

– performing measurements with a reference meter to verify the obtained results.

Due to the complexity of the issue, the work was divided into three main parts. In the Methods and Materials Section, a schematic diagram of the measurement system is defined, its operation and its cooperating elements are described. For initial calibration, the developed model was based on regression with the use of machine learning methods.

The result and discussion section presents the indications of the developed measurement system which were compared with the corresponding values from the reference meter with the use of bihistograms, the Two-Sample Kolmogorov–Smirnov test, the Bag of Words, and the Bag of Patterns [25, 26]. This is preceded by an introduction that determines the significance of the problem and the cited state of the literature emphasizes its modernity and relevance. The research results were concluded in the summary.

## 2. Method and Materials

Based on the literature, it was found that the issue of monitoring electromagnetic field in the aircraft cabin is particularly important due to the extensive use of radio navigation equipment and other on-board systems that are sources of the field. The authors have been since 2018 conducting research on the influence of electromagnetic field during, among others, training flights at the Aviation Centre of the University College of Applied Sciences in Chełm, Poland [20, 21]. This study is a continuation of the research described in [19–22]. Creation of a new, relatively cheap, compact measurement system for measuring the electrical component of the electromagnetic field was suggested. Figure 1 shows the developed measurement system. All test flights were performed in similar weather conditions. The flights were carried out on paved runway at the Depultycze Królewskie airfield near Chełm in eastern of Poland from 7.00 am to 7.00 pm UTC (Coordinated Universal Time) time. Air temperature was approximately 7–15°C. The wind direction at the ground level was between 210 and 240 degrees, the wind speed was between 6–7.5 m per second and the pressure was 1011–1016 hPa.

### *2.1. Development of the Measurement System*

The purpose of the created measurement system is to collect measurement data of the electric component of electromagnetic field. The device uses a set of 3 antennas from which the signal is transmitted to the power detector, then at the microcontroller level the signal is converted from analog to digital and the readings from the 3 antennas are averaged, the final results are displayed in a smartphone to which the device is connected via a type C USB cable. The schematic diagram of the measurement system is shown in Figures 1 through 3.

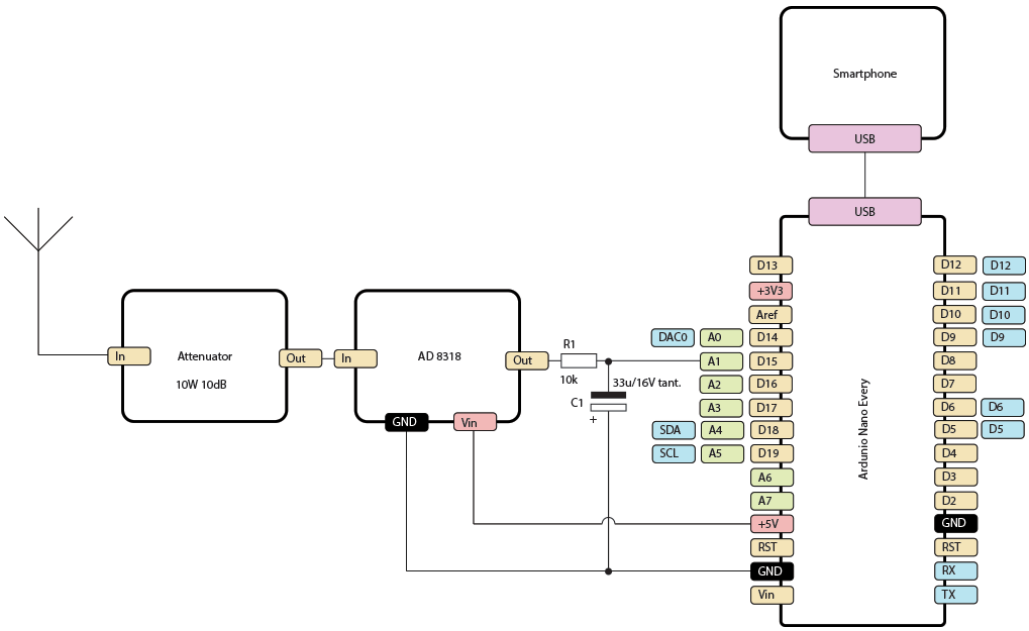


Fig. 1. Schematic diagram of the developed low-cost measurement system to measure the electric component of electromagnetic field.

*Metrol. Meas. Syst.*, Vol. 31 (2024), No. 3, pp. 577–594
DOI: 10.24425/mms.2024.150289

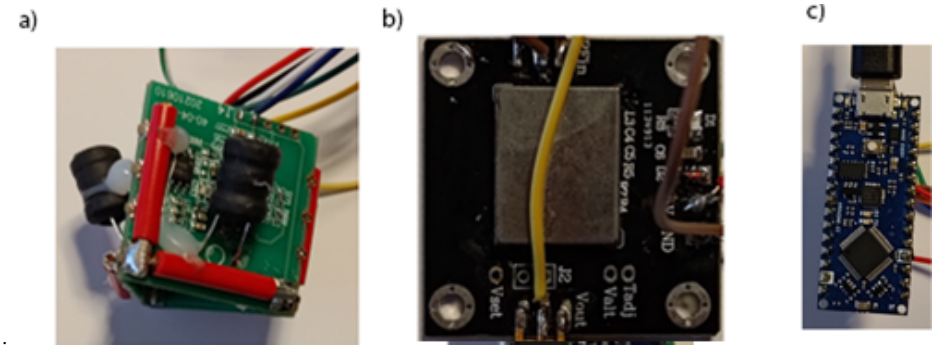


Fig. 2. Functional components of the measurement system (a) antenna, (b) power detector and (c) microcontroller board.

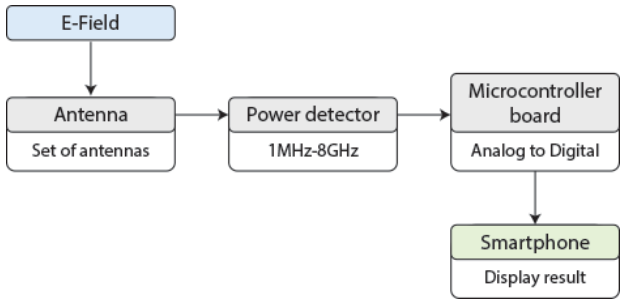


Fig. 3. The functional block diagram of the proposed measurement system to measure electric field.

The used power detector has the measurement range from 1–8000 MHz for −58 . . . − 1 dBm, which translates into 280 µV to 200 mV for 50 Ω. By using an attenuator, the measurement range can be extended to approximately 40 dBm, which translates into 10 W. Due to the need to limit the measurement band to the selected frequencies, low-pass RC filters were used in the sensor antenna circuit [25]. The developed measurement system uses an AD8318 Logarithmic Detector in combination with an Arduino microcontroller board. The microcontroller is responsible for sending data to the smartphone. The article examines regression models using Python with the scikit-learn, lightgbm and xgboost libraries.

The resolution of the ADC (Analog to Digital Converter) is 10 bits, so the values are within the range of $0–2^{10}$-1, in other words from $0^{th}$ to $1023^{rd}$ quanta. For the calibration purposes, it was decided to use an industrial grade EMF meter with a probe (reference), which provides real ground data to the machine learning model.

### *2.2. Calibration of the Measuring System*

The initial calibration of the measurement system was carried out using the reference meter (Microrad NHT3DL). The reference meter uses an 01E measurement probe. The probe is commonly used to sense both CW (*continuous wave*) and modulated signals in the frequency range from 100 kHz to 6.5 GHz. A detailed description of the reference meter specifications is presented in [20].

The calibration was performed in a GTEM 1000 (*Gigahertz Transverse Electromagnetic*) chamber with ITS 6006 generator made by Teseq (Fig. 4). The chamber is a shielded measurement environment without external sources. The shielding effectiveness for the measurement range

from 80 MHz to 6 GHz, in which the tests were performed, is more than 60 dB. ITS 6006 is a RF (*Radio Frequency*) signal generator in the range from 80 MHz to 6 GHz. The Teseq ITS 6006 consists of an integrated RF signal generator, RF switch and EUT (*Equipment Under Test*) monitoring interfaces. The signal is directly connected to a CBA 1G-070 power amplifier also made by Teseq. The computer with the WIN 6000 software installed controls the entire system of signal generation and monitoring of RF fields in the shielded chamber. Electric fields were simulated in the laboratory conditions shown in Fig. 4. The calibration of the system was carried out in electric fields of 1 V/m, 3 V/m and 10 V/m. During calibration, the tested devices were uniformly exposed to the generated electric field with set values.

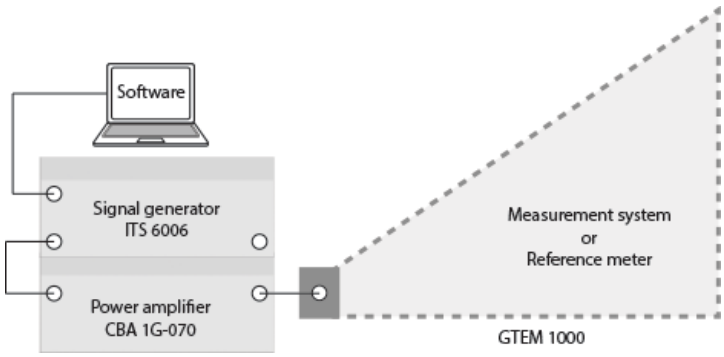


Fig. 4. Schematic diagram of initial calibration.

In order to eliminate the interaction between the reference meter and the measurement system, the calibration process was performed under the same conditions in the shielded GTEM 1000 chamber, but the measurement system was placed separately.

### *2.2.1. Calibration Using Machine Learning Models*

In order to calibrate the system, measurements were made in the chamber with the wave generator. The reference meter and the developed system were placed in the chamber separately. The time series of the readings of both devices were averaged to obtain a generalized characteristic of each device. The obtained readings were compared with each other using machine learning algorithms. The calibration procedure is presented in Fig. 5.

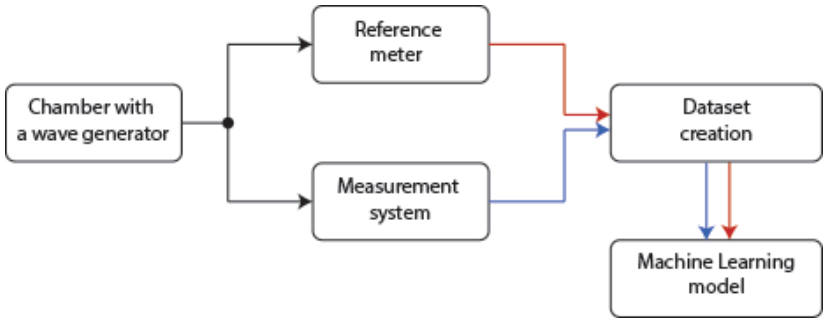


Fig. 5. Calibration process.

### *2.3. Model Selection*

In order to select the model, we focus on the machine learning solutions. Due to the character of the data, solutions based on supervised learning were selected. In machine learning supervised learning is a technique used to train a model based on pairs of input data and desired output data. This approach lets the model learn relationships between input and output data [26].

It was decided to choose the following models to fit the data for the calibration process:

– Linear Regression – baseline model;
– *K-nearest neighbors* (KNN) regressor;
– Decision Tree Regressor;
– Decision Tree Regressor with AdaBoost (Ada Boost Regressor) [27];
– Decision Tree with Gradient Boosting (Gradient Boosting Regressor) [28].

Uniform weights are used in the KNN regression, meaning that every point makes the same contribution to the categorization. To categorize a query point, the KNN algorithm is used with Euclidean metric – (1):

$$d(x, y) = \sqrt{\sum_{i=1}^{n}(x_i - y_i)^2}, \tag{1}$$

where: $x_i$, $y_i$ are coordinates of the $i$-th point.

Regression decision trees work is based on the algorithm that divides the space of input variables into areas where the predicted values of the target variable are similar. The mean squared error was chosen as the node split criterion. This criterion uses the mean of each terminal node to minimize the L2 loss and is equivalent to variance reduction as a feature selection criterion.

The *AdaBoost* (Adaptive Boosting) algorithm is a machine learning technique that is used to build a strong classifier from a set of weak classifiers. At the first stage, the algorithm first initializes the weights $w_n^1 = \frac{1}{N}$ for a data set consisting of $N$ samples. The sequential operations listed below are carried out until the number of iterations t reaches the variable $T$, or the loss function is $L_m \leq 0.5$ [27]:

- Get the data set of size N from training data with replacement with probability $w_n^t$ for $n = 1, 2, \ldots, N$ and then fit weak learning $t$ to the resampled data and calculate the fitted values on the original dataset. The fitted values are denoted as $f^t(x_n)$.
- Observation error $L_n^t$ is calculated using the equation as follows:

$$L_n^t = \frac{|y_n - f^t(x_n)|}{\max_n\{|y_n - f^t(x_n)|\}} \tag{2}$$

  where: $y_n$ is the true value.
- The model error $L_m$ is calculated by (3):

$$L_m = \sum_{n=1}^{N} L_n^t w_n^t \tag{3}$$

- If the initial criterion is not met, then the weights are updated using (4):

$$w_n^{t+1} = \frac{w_n^t \left(\frac{L_m}{1 - L_m}\right)^{1-L_n^t}}{\sum_{n=1}^{N} w_n^t \left(\frac{L_m}{1 - L_m}\right)^{1-L_n^t}} \tag{4}$$

In the case of the gradient boosting algorithm, the model is initialized with a constant value of $F_0(x)$, which is described by (5) [28]:

$$F_0(x) = \arg\min_{\gamma} \sum_{i=1}^{n} L(y_i, \gamma) \tag{5}$$

where: $L = (y_i - \gamma)^2$, $\gamma$ is the searched value, $y_i$ is a value from the data set.

The next steps are carried out in a loop from $m = 1$ to $M$:

- Residuals are calculated as follows: $r_i = -\left[\frac{dL(y_i, F(x_i))}{dF(x_i)}\right]_{F(x)=F_{m-1}(x)}$,
- Fit the regression tree with the feature $x$ versus r and create terminal node reasons $R_j$ for $j = 1, \ldots, J$
- Compute: $\gamma_j = \arg\min_{\gamma} \sum_{x_i \in R_j} L(y_i, F_{m-1}(x_i) + \gamma)$ for $j = 1, \ldots, J$,
- Update the model: $F_m(x) = F_{m-1}(x) + \nu \sum_{j=1}^{J_m} \gamma_j \mathbf{1}\ (x \in R_j)$,

where: $\mathbf{1}(\cdot)$ is the indicator function (returns 1 if the argument is true, and 0 otherwise) [27].

Variable $\nu$ is the learning rate and its numerical value lies between 0 and 1 to control the degree of contribution of the additional tree.

To compare the performance of the models described above, we use such metrics as:

- the coefficient of determination (R2), which measures how well a statistical model predicts an outcome. The lowest possible value of $R^2$is 0 and the highest possible value is 1;
- the *mean absolute error* (MAE), which indicates the average absolute error between the values predicted by the model and the actual observed values;
- the *mean square error* (MSE), which measures the average of the squares of the errors, *i.e.*, the average squared difference between the predicted values and the actual value;
- the root *mean square error* (RMSE), which determines the average distance between the predicted values from the model and the actual values. The lower the RMSE, the better a given model is able to "fit" a dataset.

The models were optimized to obtain the highest accuracy with the minimum depth of the decision tree and the minimum number of estimators. During the optimization, parameter values were increased until a plateau was reached for the metrics' values [29].

The model based on the linear regression performed the worst, it achieved the coefficient of determination $R^2$ of 0.943 with the MAE of 0.50, MSE of 0.56, and RMSE of 0.75. Models based on decision trees achieved similar values. Among these models, the Gradient Boosting Regressor model performed best, achieving $R^2$ of 0.969 with MAE 0.39, MSE 0.30 and RMSE 0.55. The Ada Boost Regressor performed the worst among tree models, achieving $R^2$ of 0.966. Among all models, the KNN model showed the best performance, achieving $R^2$ of 0.978, MAE of 0.32, MSE of 0.22, and RMSE of 0.46. In the optimization process, the model parameters were selected so that the number of nearest neighbors is 2, the brute force method was used as the algorithm responsible for finding the nearest neighbor. This method computes distances between all pairs of points in the dataset to find the best neighbors. Table 1 presents the metrics for the analyzed models. Figure 6 shows the example of the calibration and measured values. Figure 7 shows the comparison of readings of the developed measurement system and the reference meter.

To determine the error of the model, the metric $L_{pd}$ was used in the form of average percentage difference, which is determined by (6):

$$L_{pd} = \frac{\sum \left| \frac{\hat{y}_i - y_i}{\hat{y}_i + y_i} \cdot \frac{1}{2} \right| \cdot 100\%}{N} \tag{6}$$

where: $\hat{y}_i$ is the $i$-th predicted value, $y_i$ is the $i$-th true value, $N$ is the number of samples.

*Metrol. Meas. Syst.*, Vol. 31 (2024), No. 3, pp. 577–594
DOI: 10.24425/mms.2024.150289

Table 1. Fitting results for the fixed weight factor.

| Model | $R^2$ | MAE (V/m) | MSE (V/m) | RMSE (V/m) |
|---|---|---|---|---|
| Linear Regression | 0.943 | 0.50 | 0.56 | 0.75 |
| KNN Regressor | 0.978 | 0.32 | 0.22 | 0.46 |
| Decision Tree Regressor | 0.967 | 0.37 | 0.32 | 0.57 |
| Gradient Boosting Regressor | 0.969 | 0.39 | 0.30 | 0.55 |
| AdaBoost Regressor | 0.966 | 0.44 | 0.33 | 0.58 |

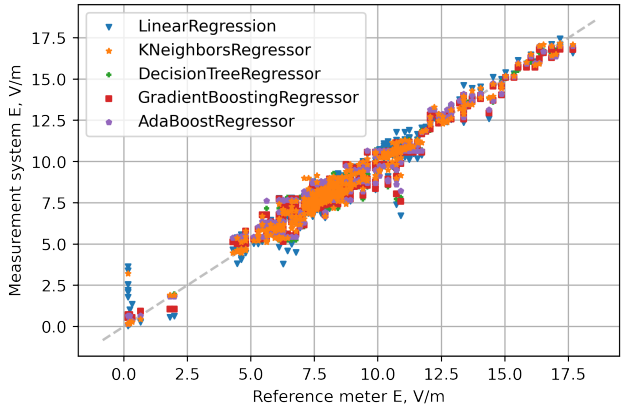


Fig. 6. Developed measurement system vs. reference meter.

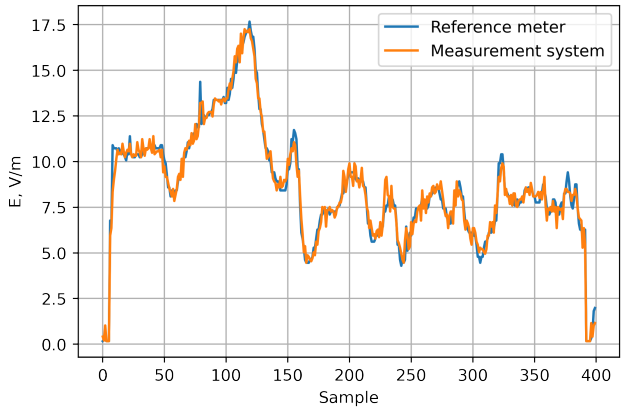


Fig. 7. Comparison of readings of the developed measurement system and the reference meter.

For the KNN regressor model, the average percentage difference is equal to 0,98%.

Also a background noise test was conducted in the chamber prior to the calibration. The average value of the noise was 0.1296 for the calibration values, and 0.1206 for the reference values. The standard deviation was 0.0126 and 0.0092 for the calibration and reference values, respectively. The minimum values were 0.1022 and 0.1000, the maximum values were 0.1663 and 0.1480 respectively.

After the calibration, the adjustment process was performed in the GTEM 1000 chamber under the electric field of $E = 10$ V/m. In order to compare the obtained results, the developed measurement system and the reference meter were placed in a shielded chamber for a 6-minute background noise test. Figure 8 shows example result of the background noise test.

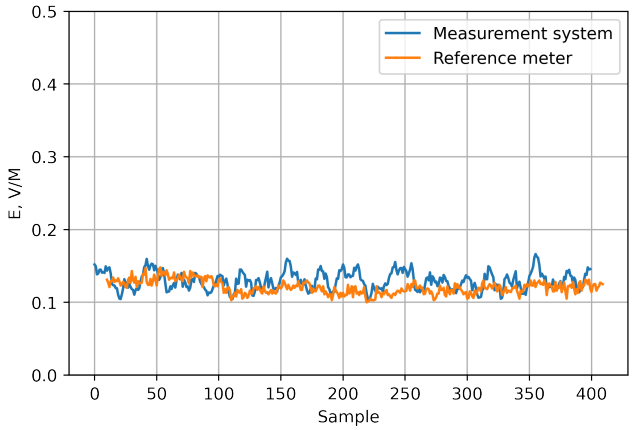


Fig. 8. Example of a background noise test.

In order to identify comparative regularities, a statistical analysis of the obtained results was carried out. Table 2 presents the results of the comparative analysis.

Table 2. Comparison of noise test for the developed system and referenced meter values (E, V/m).

| | **Developed system** | **Reference meter** |
|---|---|---|
| Mean | 0.1296 | 0.1206 |
| Standard deviation | 0.0126 | 0.0092 |
| Minimum | 0.1022 | 0.1000 |
| Maximum | 0.1663 | 0.1480 |

Based on the obtained measurements, it can be seen that the differences in the obtained average values are E = 0.009 V/m and for maximum values E = 0.0183 V/m, respectively.

## 3. Results and discussion

The tests were carried out using the developed system in a Cessna C172, an Aero AT-3 R100, a Tecnam P2006T, a PZL (State Aviation Works) M28 Bryza planes and a Mi-8 helicopter.

The system was placed in the cockpit of the test aircraft. For verification purposes, during the test flights, measurements by the reference meter were also performed. The sensor of the developed system was installed in the place occupied by the aircraft crew (see Fig. 9). It should be noted that due to the pilot's ergonomics, the selected points of installation for all aircraft were at a similar distance from the avionics instruments. At the same time, the location of the sensor did not impair safety during the test flights.

*Metrol. Meas. Syst.*, Vol. 31 (2024), No. 3, pp. 577–594
DOI: 10.24425/mms.2024.150289

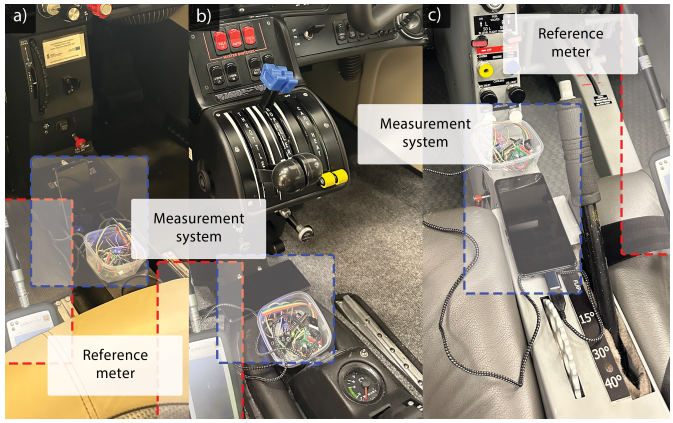


Fig. 9. Installation of the measurement system during a test flight: (a) Aero AT-3, (b) Cessna C172 and (c) Tecnam P2006T.

The results of measurements of the electric field carried out by the developed measurement system were compared with those obtained by the reference meter. Sample results are presented in this study and a detailed analysis of the measurement data obtained using the reference meter is considered in per [21].

The results were analyzed using the bihistograms and the two-sample Kolmogorov-Smirnov (KS) test. Kolmogorov–Smirnov statistics $D_{m,n}$ is determined from the equation:

$$D_{m,n} = \sup_x |F_{1,n}(x) - F_{2,m}(x)|, \tag{7}$$

where $F$ is empirical distribution functions.

In each bihistogram, one can see a similarity between the bihistogram for the tested new system (top) and for the reference meter (bottom). The KS test showed that we do not have enough evidence to reject the null hypothesis (H0) in any studied case. Thus, for each aircraft the two dataset values are from the same continuous distribution. The summary of the results of the KS test is presented in Table 3. Selected bihistograms are shown in Fig. 10.

Table 3. Results of the two-sample Kolmogorov–Smirnov test.

| **Aircraft** | **Statistic** | **p-value** | **$H_0$ rejected** |
|---|---|---|---|
| Cessna 172 | 0.0242 | 0.06972 | No |
| Aero AT-3 | 0.0161 | 0.9738 | No |
| Tecnam P2006T | 0.0223 | 0.2439 | No |

The next part of the analysis involves applying the Bag of Words (BOW) and Bag of Patterns (BOP) methods to compare signal characteristics. The BOW and BOP methods were chosen for their ability to average signal values and ignore outliers, which can lead to more stable signal characteristics. By representing a signal using a feature vector, both BOW and BOP make it easier to compare different signals and identify similarities or differences. The BOW method was applied to an averaged time series of measurements during one minute for a given route using the reference meter and the developed measurement system. BOW uses a sliding window to extract subseries, and then it uses the Piecewise Aggregate Approximation and Symbolic Aggregate Approximation

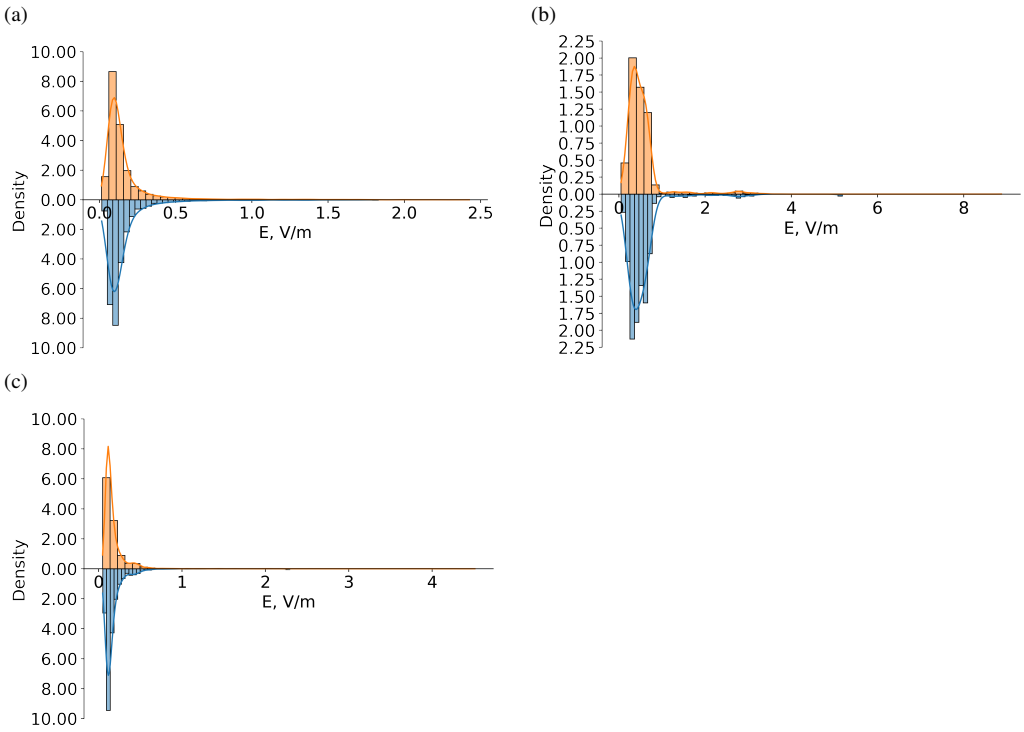


Fig. 10. Bihistogram: (a) Cessna C172, (b) Aero AT-3 and (c) Tecnam P2006T.

techniques to turn each subseries into a word. As a result, this method converts every time series into a word bag [30–33].

In the case of the Cessna 172 aircraft, in the generalized time series for one minute, there is a noticeable sequence of patterns b b b b d, c a c c c, b b b b, d b c and b d b in the time series obtained by the developed measurement system as well as by the reference meter. The aforementioned pattern sequences occur at different places in the generalized time series. This is because the measurements were made at different instants but due to the influence of various factors such as differences between flight paths the instruments' readings may have differed slightly. The plot of patterns from the BOW method are shown in Figs. 11 and 12 for the developed measurement system and for the reference meter for the Cessna C172 aircraft.

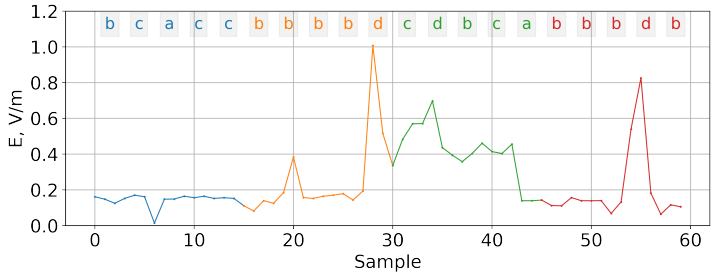


Fig. 11. BOW method for the readings of developed measurement system (Cessna 172).

*Metrol. Meas. Syst.*, Vol. 31 (2024), No. 3, pp. 577–594
DOI: 10.24425/mms.2024.150289

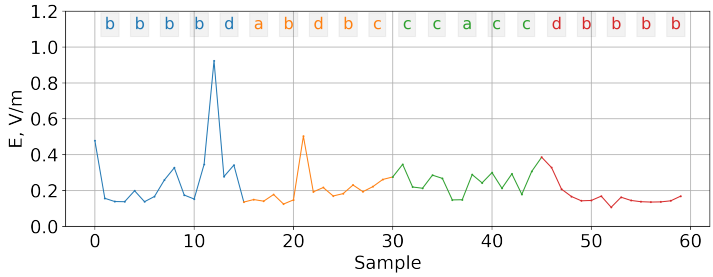


Fig. 12. BOW method for readings of reference meter (Cessna 172).

The BOP method was used to find patterns, occurring in the signals and to compare them in more depth. The BOP method is a method that works in a similar way to the BOW, except that it returns the frequencies of each word for a given time series [27]. It was decided to reduce the maximum pattern ength to 3 characters so that the method will find short but similar patterns.

In both time series for the Cessna 172 aircraft, the same patterns were found, which differ only in frequency of occurrence. For the results of the reference method, the predominant patterns are a b a and b a a, and for the developed measurement system these are a a a b. Based on the readings obtained by the developed measurement system, it can be seen that the effective value of the electric field is 1.77 V/m. Most results were within the range of 0.2–1.0 V/m. The pattern of frequency plot and measurements of the electric field performed with the developed measurement system for Cessna 172 are shown in Figure 13.

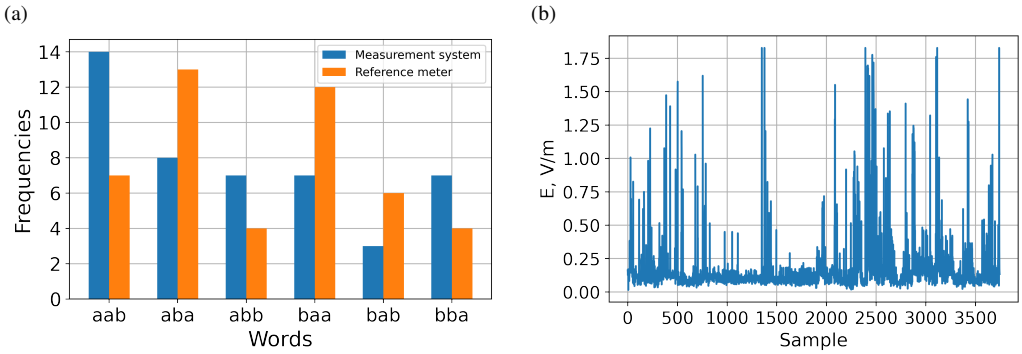


Fig. 13. Results for Cessna C172: (a) BOW method and (b) electric field measured by the developed measurement system.

In the case of Aero AT-3, the generalized time series for one minute for both the readings from the new measurement system and the reference meter exhibits the occurrence of c c b, a c c c and b b d patterns. For the patterns described above, there is a slight difference in the value of the E component. The plot of patterns for the BOW method for the developed measurement system and for the reference meter are given in Figures 14 and 15, respectively.

In both time series for the Aero AT-3 aircraft, the same patterns were found, which differ only in frequency of occurrence. In the readings, obtained on the ground by the reference meter, the predominant patterns are a a a and a b b. In the readings, obtained on the ground by the developed measurement system, the predominant patterns are b a a and b b a. In the case of Aero AT-3, it can be observed that the maximum electric field was 5.27 V/m. The range of other results obtained during the test flights is from 0.19 to 1.0 V/m. The pattern frequency plot and an example of the

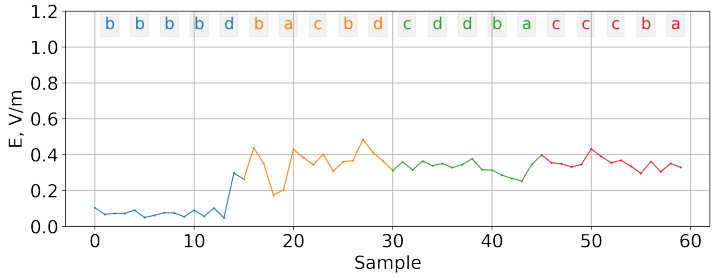


Fig. 14. BOW method for the developed measurement system (Aero AT-3).

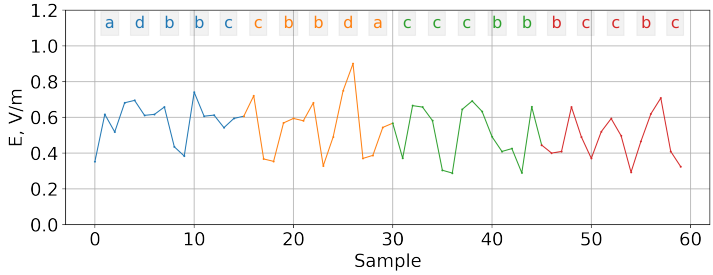


Fig. 15. BOW method for the reference meter (Aero AT-3).

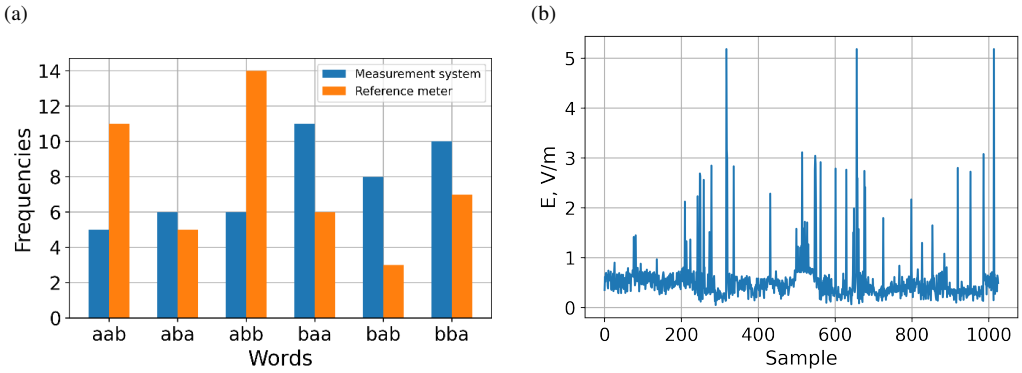


Fig. 16. Results for Aero AT-3 aircraft: (a) BOW method, (b) electric field measured by the developed measurement system.

electric field measured by the developed measurement system for the Aero AT-3 aircraft are shown in Figure 16. (błąd numeracji rysunków)

The BOW method for the generalized time series for the Tecnam P 2006T aircraft exhibits patterns d c b, b b d, a b b b, c b b, b b b d c and d c b b for the developed measurement system and the reference meter, respectively.

The BOP method for the readings of the developed measurement system as well as for the reference meter did not show the appearance of pattern a a a. The frequency pattern and the electric field measured by the developed measurement system for the Tecnam P2006T aircraft are shown in Figure 17.

*Metrol. Meas. Syst.*, Vol. 31 (2024), No. 3, pp. 577–594
DOI: 10.24425/mms.2024.150289

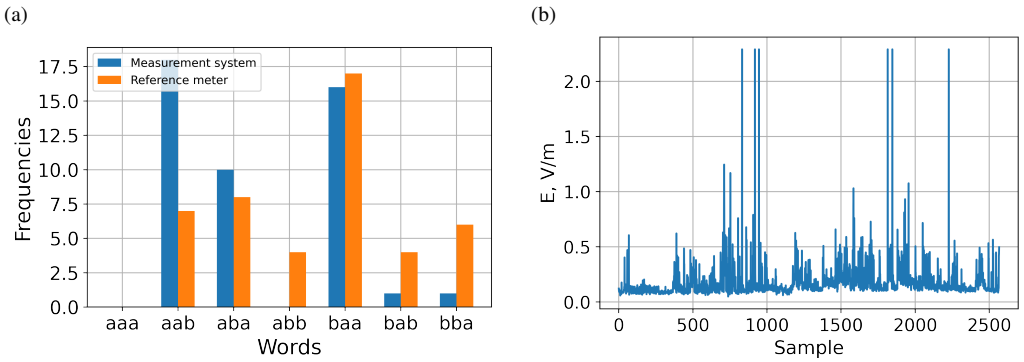


Fig. 17. Results for the Tecnam P2006T aircraft: (a) BOW method and (b) electric field measured by the developed measurement system.

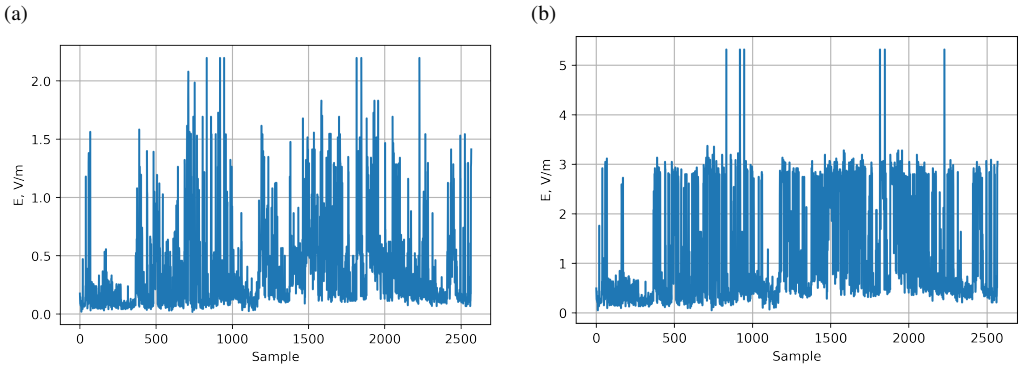


Fig. 18. Electric field measured by the developed measurement system in: (a) Mi-8 helicopter, (b) PZL M28 Bryza aircraft.

The described method was also tested on a Mi-8 helicopter and a PZL M28 Bryza plane (see Fig. 18a). The maximum reading for the MI 8 aircraft is 2.4 V/m. Most of the remaining results are within the range of 0.1-1.5 V/m. The maximum reading observed for the PZL M28 Bryza airplane was E = 5.31 V/m. It can be observed that most of the remaining measurements are between 0.1 V/m and 3.1 V/m (see Fig. 18b).

Having compared the obtained values with the guidelines included in Directive 2013/35/EU [34], we can conclude the observed electric fields in the aircrafts and helicopters do not exceed the maximum permissible level. We used a broadband device, therefore we compared the measurements with the maximum permissible level of 28 V/m, taken from the Directive 2013/35/EU.

## 4. Conclusions

The new portable low-cost measurement system to measure electric field was developed. The calibration was performed using the NHT3DL reference meter. The calibration procedure was developed using several artificial neural network models. The model based on the KNN regressor was chosen because it showed the highest accuracy among the tested models. The accuracy of the calibration using the decision tree model is confirmed by the high consistency between the measurements taken by the developed measurement system and the reference meter.

The differences between the average measurements taken by the developed measurement system and the reference meter were less than 1%. The accuracy of the obtained results is satisfactory. The developed measurement system is cheaper that the professional measurement systems while its accuracy is comparable. It can be used widely used, *e.g.* in a matrix system.

The authors plan to conduct further research with a number of measurement systems located at various points of an aircraft in order to determine which components come from the aircraft and which come from sources in the external anthropogenic environment. Further experimental studies will also be carried out to quantify any factors influencing field values.

***Acknowledgements***

Podziekowania

**References**

[1] Irfan, M., Ayub, N., Althobiani, F., Ali, Z., Idrees, M., Ullah, S., Rahman, S., Saeed Alwadie, A., Mohammed Ghonaim, S., Abdushkour, H., Salem Alkahtani, F., Alqhtani, S., & Gas, P. (2022). Energy Theft Identification Using Adaboost Ensembler in the Smart Grids. *Computers, Materials & Continua*, *72*(1), 2141–2158. https://doi.org/10.32604/cmc.2022.025466

[2] Wyszkowska, J., Maliszewska, J., & Gas, P. (2023). Metabolic and Developmental Changes in Insects as Stress-Related Response to Electromagnetic Field Exposure. *Applied Sciences*, *13*(17), 9893. https://doi.org/10.3390/app13179893

[3] Vasylkiv, N., Kochan, O., Kochan, R., & Chyrka, M. (2009, September). The control system of the profile of temperature field. *2009 IEEE International Workshop on Intelligent Data Acquisition and Advanced Computing Systems: Technology and Applications*. 2009 IEEE International Workshop on Intelligent Data Acquisition and Advanced Computing Systems: Technology and Applications (IDAACS). https://doi.org/10.1109/idaacs.2009.5342994

[4] Su, J., Beshley, M., Przystupa, K., Kochan, O., Rusyn, B., Stanisławski, R., Yaremko, O., Majka, M., Beshley, H., Demydov, I., Pyrih, J., & Kahalo, I. (2022). 5G multi-tier radio access network planning based on Voronoi diagram. *Measurement*, *192*, 110814. https://doi.org/10.1016/j.measurement.2022.110814

[5] Petroulakis, N., Mattsson, M.-O., Chatziadam, P., Simko, M., Gavrielides, A., Yiorkas, A. M., Zeni, O., Scarfi, M. R., Soudah, E., Otin, R., Schettino, F., Migliore, M. D., Miaoudakis, A., Spanoudakis, G., Bolte, J., Korkmaz, E., Theodorou, V., Zarogianni, E., Lagorio, S., ... Bogdanova, A. (2023). NextGEM: Next-Generation Integrated Sensing and Analytical System for Monitoring and Assessing Radiofrequency Electromagnetic Field Exposure and Health. *International Journal of Environmental Research and Public Health*, *20*(12), 6085. https://doi.org/10.3390/ijerph20126085

[6] Mallik, M., Tesfay, A. A., Allaert, B., Kassi, R., Egea-Lopez, E., Molina-Garcia-Pardo, J.-M., Wiart, J., Gaillot, D. P., & Clavier, L. (2022). Towards Outdoor Electromagnetic Field Exposure Mapping Generation Using Conditional GANs. *Sensors*, *22*(24), 9643. https://doi.org/10.3390/s22249643

[7] da L. A. Silva, J., de Sousa, V. A., Jr., Rodrigues, M. E. C., Pinheiro, F. S. R., da Silva, G. S., Mendonça, H. B., de F. H. Silva, R. Q., da Silva, J. V. L., Galdino, F. E. S., de Carvalho, V. F. C., & Medeiros, L. I. C. (2023). Human Exposure to Non-Ionizing Radiation from Indoor Distributed Antenna System: Shopping Mall Measurement Analysis. *Sensors*, *23*(10), 4579. https://doi.org/10.3390/s23104579

[8] Bae, H., & Park, S. (2022). Assessment of the Electromagnetic Radiation Exposure at EV Charging Facilities. *Sensors*, *23*(1), 162. https://doi.org/10.3390/s23010162

[9] Atanasova, G. L., Atanasov, B. N., & Atanasov, N. T. (2023). Assessment of Electromagnetic Field Exposure on European Roads: A Comprehensive in situ Measurement Campaign. *Sensors*, *23*(13), 6050. https://doi.org/10.3390/s23136050

[10] Zeng, Y., Qin, Y., Yang, Y., & Lu, X. (2022). A Low-Cost Flexible Capacitive Pressure Sensor for Health Detection. *IEEE Sensors Journal*, *22*(8), 7665–7673. https://doi.org/10.1109/jsen.2022.3158354

[11] Ali, S., Glass, T., Parr, B., Potgieter, J., & Alam, F. (2021). Low Cost Sensor with IoT LoRaWAN Connectivity and Machine Learning-Based Calibration for Air Pollution Monitoring. *IEEE Transactions on Instrumentation and Measurement*, *70*, 1–11. https://doi.org/10.1109/tim.2020.3034109

[12] Das, P., Ghosh, S., Chatterjee, S., & De, S. (2022). A Low Cost Outdoor Air Pollution Monitoring Device with Power Controlled Built-In PM Sensor. *IEEE Sensors Journal*, *22*(13), 13682–13695. https://doi.org/10.1109/jsen.2022.3175821

[13] Placidi, P., Vergini, C. V. D., Papini, N., Cecconi, M., Mezzanotte, P., & Scorzoni, A. (2023). Low-Cost and Low-Frequency Impedance Meter for Soil Water Content Measurement in the Precision Agriculture Scenario. *IEEE Transactions on Instrumentation and Measurement*, *72*, 1–13. https://doi.org/10.1109/tim.2023.3302898

[14] Walczak, M., Bychto, L., Kraśniewski, J., & Duer, S. (2022). Design and evaluation of a low-cost solar simulator and measurement system for low-power photovoltaic panels. *Metrology and Measurement Systems*, *29*(4), 685–700. https://doi.org/10.24425/mms.2022.143067

[15] Jakubowski, J. (2020) A study on the calibration of an HPM meter based on a D-dot sensor and logarithmic RF power detector. *Metrology and Measurement Systems, 27*(4), 673-685. https://doi.org/10.24425/mms.2020.134846

[16] Liu, C., Zhao, C., Wang, Y., & Wang, H. (2023). Machine-Learning-Based Calibration of Temperature Sensors. *Sensors*, *23*(17), 7347. https://doi.org/10.3390/s23177347

[17] Wang, A., Machida, Y., deSouza, P., Mora, S., Duhl, T., Hudda, N., Durant, J. L., Duarte, F., & Ratti, C. (2023). Leveraging machine learning algorithms to advance low-cost air sensor calibration in stationary and mobile settings. *Atmospheric Environment*, *301*, 119692. https://doi.org/10.1016/j.atmosenv.2023.119692

[18] Park, D., Yoo, G.-W., Park, S.-H., & Lee, J.-H. (2021). Assessment and Calibration of a Low-Cost PM2.5 Sensor Using Machine Learning (HybridLSTM Neural Network): Feasibility Study to Build an Air Quality Monitoring System. *Atmosphere*, *12*(10), 1306. https://doi.org/10.3390/atmos12101306

[19] Pytka, J. A., Budzyński, P., Tomiło, P., Michałowska, J., Gnapowski, E., Błażejczak, D., & Łukaszewicz, A. (2021). IMUMETER - A Convolution Neural Network-Based Sensor for Measurement of Aircraft Ground Performance. *Sensors*, *21*(14), 4726. https://doi.org/10.3390/s21144726

[20] Michałowska, J., Pytka, J., Tofil, A., Krupski, P., & Puzio, Ł. (2021). Assessment of Training Aircraft Crew Exposure to Electromagnetic Fields Caused by Radio Navigation Devices. *Energies*, *14*(1), 254. https://doi.org/10.3390/en14010254

[21] Michałowska, J., Tofil, A., Józwik, J., Pytka, J., Legutko, S., Siemiątkowski, Z., & Łukaszewicz, A. (2019). Monitoring the Risk of the Electric Component Imposed on a Pilot During Light Aircraft Operations in a High-Frequency Electromagnetic Field. *Sensors*, *19*(24), 5537. https://doi.org/10.3390/s19245537

[22] Pytka, J., Budzyński, P., Tomiło, P., Michałowska, J., Błażejczak, D., Gnapowski, E., Pytka, J., & Gierczak, K. (2022). Measurement of aircraft ground roll distance during takeoff and landing on a grass runway. *Measurement*, *195*, 111130. https://doi.org/10.1016/j.measurement.2022.111130

[23] Lin, J., Keogh, E., Wei, L., & Lonardi, S. (2007). Experiencing SAX: a novel symbolic representation of time series. *Data Mining and Knowledge Discovery*, *15*(2), 107–144. https://doi.org/10.1007/s10618-007-0064-z

[24] Keogh, E., Chakrabarti, K., Pazzani, M., & Mehrotra, S. (2001). Dimensionality Reduction for Fast Similarity Search in Large Time Series Databases. *Knowledge and Information Systems*, *3*(3), 263–286. https://doi.org/10.1007/pl00011669

[25] Bienkowski, P., & Trzaska, H. (2012). *Electromagnetic Measurements in the Near Field*. (2E) Institution of Engineering and Technology. https://doi.org/10.1049/sbew042e

[26] Chen, X., Przystupa, K., Ye, Z., Chen, F., Wang, C., Liu, J., Gao, R., Wei, M., & Kochan, O. (2022). Forecasting short-term electric load using extreme learning machine with improved tree seed algorithm based on Lévy flight. *Eksploatacja i niezawodność – Maintenance and Reliability*, *24*(1), 153–162. https://doi.org/10.17531/ein.2022.1.17

[27] Friedman, J. H. (2001). Greedy function approximation: A gradient boosting machine. *The Annals of Statistics*, *29*(5). https://doi.org/10.1214/aos/1013203451

[28] Li, Y., Wang, J., Zhang, T., Hu, H., & Wu, H. (2022). Parameter identification approach using improved teaching and learning based optimization for hub motor considering temperature rise. *Metrology and Measurement Systems*, *30*(1), 99–115. https://doi.org/10.24425/mms.2023.144396

[29] Gil, F., Osowski, S., Świderski, B., Słowińska, M. (2023). Deep learning classification and recognition method for milling surface roughness combined with simulation data. *Metrology and Measurement Systems, 30*(1),139-156. https://doi.org/10.24425/mms.2023.144400

[30] Faouzi, J., Janati, H. (2020). A Python package for time series classification. *Journal of Machine Learning Research*, 21(46), 1−6.

[31] Xiong, G., Przystupa, K., Teng, Y., Xue, W., Huan, W., Feng, Z., Qiong, X., Wang, C., Skowron, M., Kochan, O., & Beshley, M. (2021). Online Measurement Error Detection for the Electronic Transformer in a Smart Grid. *Energies*, *14*(12), 3551. https://doi.org/10.3390/en14123551

[32] Chengsheng, T., Huacheng, L., & Bing, X. (2017). AdaBoost typical algorithm and its application research. *MATEC Web of Conferences*, *139*, 00222. https://doi.org/10.1051/matecconf/201713900222

[33] Sun, L., Qin, H., Przystupa, K., Majka, M., & Kochan, O. (2022). Individualized Short-Term Electric Load Forecasting Using Data-Driven Meta-Heuristic Method Based on LSTM Network. *Sensors*, *22*(20), 7900. https://doi.org/10.3390/s22207900

[34] European Union. (2013). Directive No. 2013/35/EU of the European Parliament and of the Council of 26 June 2013, on the Minimum Health and Safety Requirements Regarding the Exposure of Workers to the Risks Arising from Physical Agents (Electromagnetic Fields). *Official Journal of the European Union*. L179, 1–21. http://eur-lex.europa.eu/legal-content/EN/TXT/PDF/?uri=CELEX:32013L0035{&}from=PT

**Joanna Michałowska** received his Ph.D. degree from Lublin University of Technology, Poland, in 2013. She is currently an Assistant Professor at the Institute of Technical Sciences and Aviation, University College of Applied Science in Chełm, Poland. She has authored or coauthored 2 book chapters, over 30 journal and 18 conference publications. Her research activity focuses on electromagnetic fields, sensors and artificial neural network.

**Paweł Tomiło** received his Ph.D. degree from Lublin University of Technology, Poland, in 2023. He is currently an Assistant Professor at the Department of Quantitative Methods in Management at Lublin University of Technology. He has authored or coauthored 8 journal and 7 conference publications. His research activity focuses on machine learning, neuroscience and mechanical engineering.